Research Article | Vol. 25, No. 2 | 23 Jan 2017 | OPTICS EXPRESS 1381

Optics EXPRESS

Droop-free $Al_xGa_{1-x}N/Al_yGa_{1-y}N$ quantum-disks-in-nanowires ultraviolet LED emitting at 337 nm on metal/silicon substrates

Bilal Janjua,[1,5] Haiding Sun,[2,5] Chao Zhao,[1] Dalaver H. Anjum,[3] Davide Priante,[1] Abdullah A. Alhamoud,[1,4] Feng Wu,[2] Xiaohang Li,[2] Abdulrahman M. Albadri,[4] Ahmed Y. Alyamani,[4] Munir M. El-Desouki,[4] Tien Khee Ng,[1] Boon S. Ooi[1,*]

[1]*King Abdullah University of Science and Technology (KAUST), Photonics Laboratory, Thuwal 23955-6900, Saudi Arabia*
[2]*King Abdullah University of Science and Technology (KAUST), Advanced Semiconductor Laboratory, Thuwal 23955-6900, Saudi Arabia*
[3]*King Abdullah University of Science and Technology (KAUST), Imaging and Characterization Core Lab, Thuwal 23955-6900, Saudi Arabia*
[4]*National Center for Nanotechnology, King Abdulaziz City for Science and Technology (KACST), Riyadh, 11442-6086, Saudi Arabia*
[5]*These authors contributed equally to this work*
[*]*boon.ooi@kaust.edu.sa*

Abstract: Currently the AlGaN-based ultraviolet (UV) solid-state lighting research suffers from numerous challenges. In particular, low internal quantum efficiency, low extraction efficiency, inefficient doping, large polarization fields, and high dislocation density epitaxy constitute bottlenecks in realizing high power devices. Despite the clear advantage of quantum-confinement nanostructure, it has not been widely utilized in AlGaN-based nanowires. Here we utilize the self-assembled nanowires (NWs) with embedding quantum-disks (Qdisks) to mitigate these issues, and achieve UV emission of 337 nm at 32 A/cm^2 (80 mA in 0.5 × 0.5 mm^2 device), a turn-on voltage of ~5.5 V and droop-free behavior up to 120 A/cm^2 of injection current. The device was grown on a titanium-coated n-type silicon substrate, to improve current injection and heat dissipation. A narrow linewidth of 11.7 nm in the electroluminescence spectrum and a strong wavefunctions overlap factor of 42% confirm strong quantum confinement within uniformly formed AlGaN/AlGaN Qdisks, verified using transmission electron microscopy (TEM). The nitride-based UV nanowires light-emitting diodes (NWs-LEDs) grown on low cost and scalable metal/silicon template substrate, offers a scalable, environment friendly and low cost solution for numerous applications, such as solid-state lighting, spectroscopy, medical science and security.

OCIS codes: (230.3670) Light-emitting diodes; (230.5590) Quantum-well, -wire and -dot devices; (160.3900) Metals; (160.6000) Semiconductor materials; (260.7190) Ultraviolet.

References and links

1. A. Khan, K. Balakrishnan, and T. Katona, "Ultraviolet light-emitting diodes based on group three nitrides," Nat. Photonics **2**(2), 77–84 (2008).
2. S.-H. Park and S.-L. Chuang, "Crystal-orientation effects on the piezoelectric field and electronic properties of strained wurtzite semiconductors," Phys. Rev. B **59**(7), 4725–4737 (1999).
3. S.-H. Park and S.-L. Chuang, "Comparison of zinc-blende and wurtzite GaN semiconductors with spontaneous polarization and piezoelectric field effects," J. Appl. Phys. **87**(1), 353–364 (2000).
4. S.-H. Park, "Crystal orientation effects on electronic properties of wurtzite GaN/AlGaN quantum wells with spontaneous and piezoelectric polarization," Jpn. J. Appl. Phys. **39**(Part 1, No. 6A), 3478–3482 (2000).
5. J. Piprek, *Nitride Semiconductor Devices: Principles and Simulation* (John Wiley & Sons, 2007).
6. O. Ambacher, "Growth and applications of group III-nitrides," J. Phys. D Appl. Phys. **31**(20), 2653–2710 (1998).

#281113 http://dx.doi.org/10.1364/OE.25.001381
Journal © 2017 Received 21 Nov 2016; revised 11 Jan 2017; accepted 12 Jan 2017; published 18 Jan 2017

Optics EXPRESS

7. M. Shatalov, W. H. Sun, A. Lunev, X. H. Hu, A. Dobrinsky, Y. Bilenko, J. W. Yang, M. Shur, R. Gaska, C. Moe, G. Garrett, and M. Wraback, "AlGaN deep-ultraviolet light-emitting diodes with external quantum efficiency above 10%," Appl. Phys. Express **5**(8), 082101 (2012).
8. M. Kneissl and J. Rass, *III-Nitride Ultraviolet Emitters: Technology and Applications* (Springer, 2015).
9. M. Kneissl, T. Kolbe, C. Chua, V. Kueller, N. Lobo, J. Stellmach, A. Knauer, H. Rodriguez, S. Einfeldt, Z. Yang, N. M. Johnson, and M. Weyers, "Advances in group III-nitride-based deep UV light-emitting diode technology," Semicond. Sci. Technol. **26**(1), 014036 (2011).
10. Q. Wang, S. Zhao, A. T. Connie, I. Shih, Z. Mi, T. Gonzalez, M. P. Andrews, X. Z. Du, J. Y. Lin, and H. X. Jiang, "Optical properties of strain-free AlN nanowires grown by molecular beam epitaxy on Si substrates," Appl. Phys. Lett. **104**, 4881558 (2014).
11. M. Djavid and Z. T. Mi, "Enhancing the light extraction efficiency of AlGaN deep ultraviolet light emitting diodes by using nanowire structures," Appl. Phys. Lett. **108**(5), 051102 (2016).
12. Q. Wang, H. P. T. Nguyen, K. Cui, and Z. Mi, "High efficiency ultraviolet emission from AlxGa1-xN core-shell nanowire heterostructures grown on Si (111) by molecular beam epitaxy," Appl. Phys. Lett. **101**, 4738983 (2012).
13. R. Calarco, R. J. Meijers, R. K. Debnath, T. Stoica, E. Sutter, and H. Lüth, "Nucleation and growth of GaN nanowires on Si(111) performed by molecular beam epitaxy," Nano Lett. **7**(8), 2248–2251 (2007).
14. B. J. May, A. T. M. G. Sarwar, and R. C. Myers, "Nanowire LEDs grown directly on flexible metal foil," Appl. Phys. Lett. **108**(14), 141103 (2016).
15. M. Yoshizawa, A. Kikuchi, M. Mori, N. Fujita, and K. Kishino, "Growth of self-organized GaN nanostructures on Al2O3(0001) by RF-radical source molecular beam epitaxy," Jpn. J. Appl. Phys. **2**(36), L459–L462 (1997).
16. M. Wölz, C. Hauswald, T. Flissikowski, T. Gotschke, S. Fernández-Garrido, O. Brandt, H. T. Grahn, L. Geelhaar, and H. Riechert, "Epitaxial growth of GaN nanowires with high structural perfection on a metallic TiN film," Nano Lett. **15**(6), 3743–3747 (2015).
17. S. Inoue, K. Okamoto, T. Nakano, J. Ohta, and H. Fujioka, "Epitaxial growth of AlN films on Rh ultraviolet mirrors," Appl. Phys. Lett. **91**(13), 131910 (2007).
18. S. Zhao, M. Djavid, and Z. Mi, "Surface emitting, high efficiency near-vacuum ultraviolet light source with aluminum nitride nanowires monolithically grown on silicon," Nano Lett. **15**(10), 7006–7009 (2015).
19. Z. T. Mi, S. R. Zhao, A. Connie, M. Hadi, and T. Dastjerdi, "High efficiency AlGaN deep ultraviolet light emitting diodes on silicon," Proc. SPIE **9373**, 937306 (2015).
20. Q. Wang, A. T. Connie, H. P. T. Nguyen, M. G. Kibria, S. Zhao, S. Sharif, I. Shih, and Z. Mi, "Highly efficient, spectrally pure 340 nm ultraviolet emission from AlxGa1-xN nanowire based light emitting diodes," Nanotechnology **24**(34), 345201 (2013).
21. A. T. M. G. Sarwar, B. J. May, J. I. Deitz, T. J. Grassman, D. W. McComb, and R. C. Myers, "Tunnel junction enhanced nanowire ultraviolet light emitting diodes," Appl. Phys. Lett. **107**(10), 101103 (2015).
22. H. Sekiguchi, K. Kato, J. Tanaka, A. Kikuchi, and K. Kishino, "Ultraviolet GaN-based nanocolumn light-emitting diodes grown on n-(111) Si substrates by rf-plasma-assisted molecular beam epitaxy," Phys. Status Solidi., A Appl. Mater. Sci. **205**(5), 1067–1069 (2008).
23. D. S. Shin, D. P. Han, J. Y. Oh, and J. I. Shim, "Study of droop phenomena in InGaN-based blue and green light-emitting diodes by temperature-dependent electroluminescence," Appl. Phys. Lett. **100**(15), 153506 (2012).
24. K. C. Yung, H. Liem, H. S. Choy, and W. K. Lun, "Degradation mechanism beyond device self-heating in high power light-emitting diodes," J. Appl. Phys. **109**(9), 094509 (2011).
25. C. Zhao, T. K. Ng, N. Wei, A. Prabaswara, M. S. Alias, B. Janjua, C. Shen, and B. S. Ooi, "Facile formation of high-quality InGaN/GaN quantum-disks-in-nanowires on bulk-metal substrates for high-power light-emitters," Nano Lett. **16**(2), 1056–1063 (2016).
26. A. T. M. G. Sarwar, S. D. Carnevale, F. Yang, T. F. Kent, J. J. Jamison, D. W. McComb, and R. C. Myers, "Semiconductor nanowire light-emitting diodes grown on metal: a direction toward large-scale fabrication of nanowire devices," Small **11**(40), 5402–5408 (2015).
27. W. M. Rohsenow and H. Choi, *Heat Mass and Momentum Transfer* (Prentice Hall, 1961).
28. H. Yao, J. A. Woollam, and S. A. Alterovitz, "Spectroscopic ellipsometry studies of HF treated Si (100) surfaces," Appl. Phys. Lett. **62**(25), 3324–3326 (1993).
29. S. Birner, T. Zibold, T. Andlauer, T. Kubis, M. Sabathil, A. Trellakis, and P. Vogl, "nextnano: General purpose 3-D simulations," IEEE Trans. Electron Dev. **54**(9), 2137–2142 (2007).
30. C. Zhao, T. K. Ng, R. T. ElAfandy, A. Prabaswara, G. B. Consiglio, I. A. Ajia, I. S. Roqan, B. Janjua, C. Shen, J. Eid, A. Y. Alyamani, M. M. El-Desouki, and B. S. Ooi, "Droop-Free, reliable, and high-power InGaN/GaN nanowire light emitting diodes for monolithic metal-optoelectronics," Nano Lett. **16**(7), 4616–4623 (2016).
31. B. Janjua, T. K. Ng, C. Zhao, A. Prabaswara, G. B. Consiglio, D. Priante, C. Shen, R. T. ElAfandy, D. H. Anjum, A. A. Alhamoud, A. A. Alatawi, Y. Yang, A. Y. Alyamani, M. M. Eldesouki, and B. S. Ooi, "True yellow light-emitting diodes as phosphor for tunable color-rendering index laser-based white light," ACS Photonics **3**(11), 2089–2095 (2016).
32. S. D. Carnevale, T. F. Kent, P. J. Phillips, A. T. M. G. Sarwar, C. Selcu, R. F. Klie, and R. C. Myers, "Mixed polarity in polarization-induced p-n junction nanowire light-emitting diodes," Nano Lett. **13**(7), 3029–3035 (2013).

Optics EXPRESS

33. Y. Li, J. Xiang, F. Qian, S. Gradecak, Y. Wu, H. Yan, D. A. Blom, C. M. Lieber, and C. M. Lieber, "Dopant-free GaN/AlN/AlGaN radial nanowire heterostructures as high electron mobility transistors," Nano Lett. **6**(7), 1468–1473 (2006).
34. Y. T. Liao, C. Thomidis, C. K. Kao, and T. D. Moustakasa, "AlGaN based deep ultraviolet light emitting diodes with high internal quantum efficiency grown by molecular beam epitaxy," Appl. Phys. Lett. **98**(8), 081110 (2011).
35. M. Belloeil, B. Gayral, and B. Daudin, "Quantum dot-like behavior of compositional fluctuations in AlGaN nanowires," Nano Lett. **16**(2), 960–966 (2016).
36. A. Pierret, C. Bougerol, B. Gayral, M. Kociak, and B. Daudin, "Probing alloy composition gradient and nanometer-scale carrier localization in single AlGaN nanowires by nanocathodoluminescence," Nanotechnology **24**(30), 305703 (2013).
37. S. Zhao, A. T. Connie, M. H. T. Dastjerdi, X. H. Kong, Q. Wang, M. Djavid, S. Sadaf, X. D. Liu, I. Shih, H. Guo, and Z. Mi, "Aluminum nitride nanowire light emitting diodes: Breaking the fundamental bottleneck of deep ultraviolet light sources," Sci. Rep. **5**, 8332 (2015).
38. O. Landre, D. Camacho, C. Bougerol, Y. M. Niquet, V. Favre-Nicolin, G. Renaud, H. Renevier, and B. Daudin, "Elastic strain relaxation in GaN/AlN nanowire superlattice," Phys. Rev. B **81**(15), 153306 (2010).
39. J. Renard, R. Songmuang, G. Tourbot, C. Bougerol, B. Daudin, and B. Gayral, "Evidence for quantum-confined Stark effect in GaN/AlN quantum dots in nanowires," Phys. Rev. B **80**(12), 121305 (2009).
40. A. A. Darhuber, T. Grill, J. Stangl, G. Bauer, D. J. Lockwood, J. P. Noel, P. D. Wang, and C. M. S. Torres, "Elastic relaxation of dry-etched Si/SiGe quantum dots," Phys. Rev. B **58**(8), 4825–4831 (1998).
41. Z. Mi, S. Zhao, S. Y. Woo, M. Bugnet, M. Djavid, X. Liu, J. Kang, X. Kong, W. Ji, H. Guo, Z. Liu, and G. A. Botton, "Molecular beam epitaxial growth and characterization of Al(Ga)N nanowire deep ultraviolet light emitting diodes and lasers," J. Phys. D Appl. Phys. **49**(36), 364006 (2016).
42. Y. Taniyasu, M. Kasu, and T. Makimoto, "An aluminium nitride light-emitting diode with a wavelength of 210 nanometres," Nature **441**(7091), 325–328 (2006).
43. S. Zhao, S. Y. Woo, S. M. Sadaf, Y. Wu, A. Pofelski, D. A. Laleyan, R. T. Rashid, Y. Wang, G. A. Botton, and Z. Mi, "Molecular beam epitaxy growth of Al-rich AlGaN nanowires for deep ultraviolet optoelectronics," Appl. Mater. **4** (2016).
44. A. T. M. G. Sarwar, B. J. May, M. F. Chisholm, G. J. Duscher, and R. C. Myers, "Ultrathin GaN quantum disk nanowire LEDs with sub-250 nm electroluminescence," Nanoscale **8**(15), 8024–8032 (2016).
45. T. F. Kent, S. D. Carnevale, A. T. M. Sarwar, P. J. Phillips, R. F. Klie, and R. C. Myers, "Deep ultraviolet emitting polarization induced nanowire light emitting diodes with AlxGa$_1$-xN active regions," Nanotechnology **25**(45), 455201 (2014).
46. S. Zhao, X. Liu, S. Y. Woo, J. Kang, G. A. Botton, and Z. Mi, "An electrically injected AlGaN nanowire laser operating in the ultraviolet-C band," Appl. Phys. Lett. **107**(4), 043101 (2015).
47. S. D. Carnevale, T. F. Kent, P. J. Phillips, M. J. Mills, S. Rajan, and R. C. Myers, "Polarization-induced pn diodes in wide-band-gap nanowires with ultraviolet electroluminescence," Nano Lett. **12**(2), 915–920 (2012).
48. S. Zhao, S. Y. Woo, M. Bugnet, X. Liu, J. Kang, G. A. Botton, and Z. Mi, "Three-dimensional quantum confinement of charge carriers in self-organized AlGaN nanowires: a viable route to electrically injected deep ultraviolet lasers," Nano Lett. **15**(12), 7801–7807 (2015).
49. K. H. Li, X. Liu, Q. Wang, S. Zhao, and Z. Mi, "Ultralow-threshold electrically injected AlGaN nanowire ultraviolet lasers on Si operating at low temperature," Nat. Nanotechnol. **10**(2), 140–144 (2015).
50. B. H. Le, S. Zhao, X. Liu, S. Y. Woo, G. A. Botton, and Z. Mi, "Controlled coalescence of AlGaN nanowire arrays: an architecture for nearly dislocation-free planar ultraviolet photonic device applications," Adv. Mater. **28**(38), 8446–8454 (2016).
51. W. Guo, M. Zhang, P. Bhattacharya, and J. Heo, "Auger recombination in III-nitride nanowires and its effect on nanowire light-emitting diode characteristics," Nano Lett. **11**(4), 1434–1438 (2011).
52. E. Kioupakis, P. Rinke, K. T. Delaney, and C. G. Van de Walle, "Indirect Auger recombination as a cause of efficiency droop in nitride light-emitting diodes," Appl. Phys. Lett. **98**(16), 161107 (2011).
53. H. Yoshida, Y. Yamashita, M. Kuwabara, and H. Kan, "A 342-nm ultraviolet AlGaN multiple-quantum-well laser diode," Nat. Photonics **2**(9), 551–554 (2008).
54. W. Guo, M. Zhang, A. Banerjee, and P. Bhattacharya, "Catalyst-free InGaN/GaN nanowire light emitting diodes grown on (001) silicon by molecular beam epitaxy," Nano Lett. **10**(9), 3355–3359 (2010).
55. M. Knelangen, V. Consonni, A. Trampert, and H. Riechert, "In situ analysis of strain relaxation during catalyst-free nucleation and growth of GaN nanowires," Nanotechnology **21**(24), 245705 (2010).

1. Introduction

AlGaN-based ultraviolet (UV) to deep-UV (DUV) (3.5 – 6.2 eV) light emitting diodes (LED) technology is attractive for applications in environmental cleaning, medicine and lighting. It further offers compact foot-print, potentially-high efficiency, environmentally-friendly (mercury-free) features as compared to conventional UV-lamp [1]. Although progress has been remarkable for planar LEDs based on this material, such diodes based solution still exhibits low external quantum efficiency (EQE) close to 15% and far from satisfactory high

Optics EXPRESS

power operation [2–8]. A bottleneck in substrate technology in the absence of cheap substrate for AlGaN materials resulted in a high dislocation density exceeding 10^9 cm^{-2} and less than 40% internal quantum efficiency (IQE) in UV/DUV LEDs [9]. The high polarization field of several $MV \cdot cm^{-1}$ further reduced electron-hole wavefunctions overlap in the active regions, and aggravates the decrease in radiative recombination.

The AlGaN-based nanowires (NWs), on the other hand, nucleate via lateral strain relaxation and result in dislocation-free 3D structures with considerably lower piezoelectric polarization fields in the active region [10]. Mehrdad *et al.* recently reported, based on simulation work, up to 70% light extraction efficiency for NW based devices due to light scattering and reduced reabsorption [11]. Although non-radiative recombination at the surface states is one of the main causes of low IQE in InGaN-based NWs-LEDs, Z. Mi *et al.* recently reported IQE value up to 58% due to the formation of AlGaN core-shell structure which acts as a self-passivation layer and provides superior carrier confinement [12].

Furthermore, nearly dislocation-free nitride NWs have been shown to grow on a variety of substrates, e.g. Si, metal, sapphire substrates etc [13–17]. Most of the GaN-based NWs have been developed by using Si substrate as a cheap alternative. Recently Z. Mi *et al*. reported AlGaN based NWS structures emitting at 210 nm, 300 nm and 340 nm using double heterostructure (DHT) [18–20]. In parallel other group have taken an approach of using multiple GaN/AlGaN Qdisks embedded in AlGaN/AlN matrix grown on Si and used polarization enhanced doping to improve the performance of the UV LED emitting at 281, 312 and 354 nm [14, 21, 22]. However, Si-based UV LED suffers from formation of insulating amorphous Si_3N_4 nucleation layer. Lateral confinement of acoustic phonons occur due to the presence of small diameter of NWs restricting their transport to one-dimension, thus resulting in severe junction heating and even damage to the NWs devices [23, 24].

Until recently, NWs grown on metal have shown promising results for achieving high power visible light emitting devices [25]. Sarwar *et al.* were the first to show UV LED emitting at 385 nm, using GaN active region, grown on Mo film on Si wafers [26]. Moving forward, Myers group recently demonstrate an AlGaN based UV device emitting at 350 nm grown on flexible Ta film with a turn-on voltage of 5 V [14]. Utilizing Ti, which ensures formation of TiN during plasma exposure in the absence of insulating Si_3N_4 allows better heat dissipation and excellent current injection. In addition, Ti having a reflectivity of more than 35% in the UV-A regime, retains adequate light extraction efficiency thus provides a viable option for efficient UV devices [27]. Alternatively, Al being the ideal template substrate for UV back reflection, is not compatible with growth temperature for high quality AlGaN-based structures, thus requires more complicated, costly and time consuming liftoff and transfer processes.

Here we report a UV-emitting, AlGaN-quantum-disks (Qdisks)-in-NWs LED operating at room temperature. The peak emission at 337 nm was obtained at 32 A/cm^2 bias (80 mA in a 0.5×0.5 mm^2 device) with an FWHM of ~11.2 nm. The LED showed a turn-on voltage of 5.5 V which is typical for LEDs grown on n-type Si substrate emitting at similar wavelengths. Quantum confinement calculation of the Qdisks showed an overlap of 42% for the electron and hole wavefunctions using nextnano^3 software. The reduced separation of carriers is an indication of suppressed strain induced polarization fields in such 3D structures which is confirmed by the constant electroluminescence peak position with increasing current bias. The use of Qdisks-in-NW grown on ohmic TiN/Ti nucleation layer resulted in droop-free operation up to 120 A/cm^2 of injection current.

2. Experimental description

The UV NW p-i-n LED structure was grown catalyst-free using *Veeco Gen* 930 plasma assisted molecular beam epitaxy system (PAMBE) under nitrogen-rich conditions. The samples were loaded into the electron beam evaporator chamber, within less than 30 mins following HF treatment, for 100-nm Ti deposition. In Si, HF treatment results in hydrogen

Optics EXPRESS

terminated surface which resists oxide formation. Hence, further oxidation after HF cleaning is unlikely. Therefore, the time-link between HF-cleaning and Ti-deposition is very unlikely to be a determining factor on device efficiency [28]. To remove any water components, the sample was outgassed in the load lock at 200 °C using the IR filament. Outgassing at 600 °C was subsequently done in the buffer chamber to remove any organic based contaminants. The substrate was then ramped up to growth temperature. Up till the initiation of the growth, the wafer was kept away from the sources.

A 2-step growth method was adopted to nucleate high density vertically aligned NWs. NWs were first nucleated at a low temperature of 485 °C, to increase the nucleation probability, followed by growth at a higher temperature of 585 °C to improve crystal quality. Approximately ~98 nm of Si-doped GaN layer was grown. During the initial process, the formation of titanium nitride (TiN) layer at the nanowire base is expected [25]. To improve the crystal quality, the growth temperature of AlGaN layer was raised to 630 °C. The nominal Al composition was estimated by taking the ratio of Al with the total metal beam equivalent pressure (BEP) as measured by the beam flux monitor. Si-doped $Al_yGa_{1-y}N$ was then grown for ~59 nm to provide larger bandgap for quantum confinement.

An active region with 10 stacks of $Al_xGa_{1-x}N$ Qdisks separated by $Al_yGa_{1-y}N$ quantum barriers (QB), where $x < y$, were then grown on the n-AlGaN layer. For the active region, two pairs of Al and Ga sources were used with BEP set to $0.75x10^{-8}$ and $4.5x10^{-8}$ Torr for quantum wells and $1.5x10^{-8}$ and $3x10^{-8}$ Torr for quantum barriers. A ~70 nm magnesium (Mg) doped $Al_yGa_{1-y}N$ layer was then grown as the p-contact layer, keeping in mind planarization process tolerance, to avoid the shortage of device. The device was completed with a ~17 nm Mg-doped GaN layer as the p-type contact layer. For optimized NWs shape and density, nitrogen flow was maintained at 1 sccm with RF power fixed at 350 W.

The UV nanowire LEDs were fabricated using the standard UV contact lithography process. Planarization of the NWs was first done, using parylene-C, consisting of deposition step followed by the etch-back process to reveal the p-GaN contact layers. Next, to get rid of the oxide layer, the sample was dipped in buffered HF solution for 10 s. Ni (5 nm) / Au (5 nm) were deposited directly on top of p-GaN layer, which forms an ohmic contact with p-GaN, upon annealing at 600 °C under O_2 gas ambient for 1 min. The thickness of Ni/Au was adjusted to provide good current spreading, as well as being sufficiently transparent for UV light. Ni (10 nm) / Gold (Au) (500 nm) was then deposited as the top p-contact for probing. For n-contact, silicon was etched 200 nm from the back to expose clean surface. Ti (10 nm) / Au (150 nm) were then sputtered as n-pad followed by annealing in N_2 gas ambient at 250 °C for 1 min to form n-type contact.

Room Temperature Photoluminescence (RTPL) measurement was performed using a 266 nm excitation pulse laser (SNU-20F-100) in a reflective mode configuration. The PL signal was collected using a UV objective (LMU-5X-UVB) and using a beam splitter (BSW19) and then focused into the Andor monochromator (Shamrock 750). A 266 nm high pass filter (LP02-266RU-25) was used to filter off laser radiation. Signal was measured using a cooled (−80 °C) iDUS UV/VIS silicon-based CCD camera connected to the monochromator.

Electroluminescent (EL) signal was measured using PL setup with a camera attached to the beam splitter mount. A Keithley source 2450C was used to inject continuous current into the device.

Scanning electron microscopy (SEM) and scanning transmission electron microscopy (STEM) were used to investigate the quality and structure of the NWs. SEM images were taken using Nova NanoSEM 630. Whereas Titan 80-300 ST microscope (FEI Company, Hillsboro, OR) was utilized for STEM characterization. The microscope was operated at the accelerating voltage of 300 kV. Atomic-number sensitive (Z-contrast) STEM was realized by acquiring the data with High-angle annular dark-field (HAADF) detector.

The UV NWs-LEDs were modeled using the nextnano^3 software [29]. The band diagram of the structure was obtained by self-consistently solving Poisson's, Schrödinger's, current

Optics EXPRESS

continuity, and carrier transport equations. For valence band, the 6 × 6 *k.p* method was adopted to take into account non-parabolic nature of the energy bands. The effects of wavefunctions overlap, carrier dynamics in AlGaN based active region and polarization induced band bending due to interface fixed charges, were also considered.

3. Results and discussion

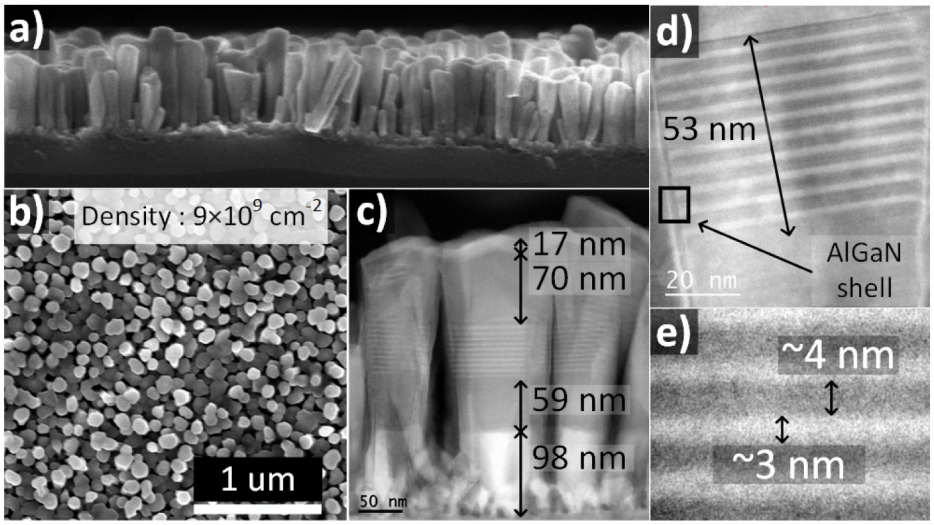

Fig. 1. Structural characterization of the NWs. (a) Cross section SEM image shows vertically aligned NWs. (b) Top view SEM image of the device grown on Ti/Si substrate shows tightly packed NWs. (c) High angle annular dark field scanning transmission electron microscopy (HAADF-STEM) of AlGaN nanowire showing the n-type AlGaN layer, AlGaN/AlGaN QDisks, p-type AlGaN, and p-GaN layer. (d) Active region is showing 10 pairs of uniform Qdisks formation. (d) Zoomed-in image of the Qdisks show compositional variation across the Qdisks.

Figure 1(a) shows NWs 70-90 nm in diameter and 300-350 nm in length. Slight height non-uniformity can come from the roughness introduced by the possible Ti and Ti/Si interface. Figure 1(b) shows top-view SEM of the NWs, being nucleated on Ti coated Si (100) substrate. TiN formation is thermodynamically favored when growing on a similar metal template substrate. The titanium layer deposited on crystalline substrate showed a preferred (0002) crystalline orientation because of it having the lowest surface energy [30]. According to Bragg's law, TiN (111), and GaN (0002) planes are parallel to each other, which is confirmed by the epitaxial growth of GaN on the TiN nucleation layer [31]. No obvious coalescence is observed. The density was estimated to be ~9 x10^9 cm^{-2}. The AlGaN NWs are expected to be N-polar as reported earlier since the NWs were grown by MBE under nitrogen-rich conditions [25, 32].

HRTEM in Fig. 1(c) shows vertical closely spaced, disjointed NWs nucleating on top of the Ti metal layer. Individual layers of the structures can be clearly distinguished in light of the varying contrast introduced by Al atoms. Figure 1(d) confirms the formation of well-defined uniform 10 $Al_xGa_{1-x}N$ Qdisks (~3.1 nm) sandwiched between $Al_yGa_{1-y}N$ (~4 nm) layers, where x < y, in the active region. Such small wavelength emission on lattice mismatched cheap substrate while maintaining good crystalline quality can only be realized in dislocation-free nanostructures [33]. Compositional variation is observed across the Qdisks which can lead to energy band fluctuations as shown in Fig. 1(e). Such fluctuation has shown to improve radiative recombination and in turn IQE [34–36]. Further examination indicates the absence of misfit dislocations and stacking faults. The NWs are seen to exhibit inverse tapered shape being thinnest at the bottom (~35 nm) and reaching a diameter of ~80 nm at the

Optics EXPRESS

top. This is due to the variation in growth temperature and slight lateral growth preference due to high Ga adatoms mobility. In particular for AlGaN based NWs, small diffusion length of aluminum promotes lateral growth thus resulting in an encapsulation/core, as seen in the marked box in Fig. 1(d) [12, 37]. The growth temperature was stabilized before initiating growth of the NWs and the active region to increase the uniformity of Qdisks. A 3D schematic of the UV NWs device is shown in Fig. 2(a) with the structure discussed earlier.

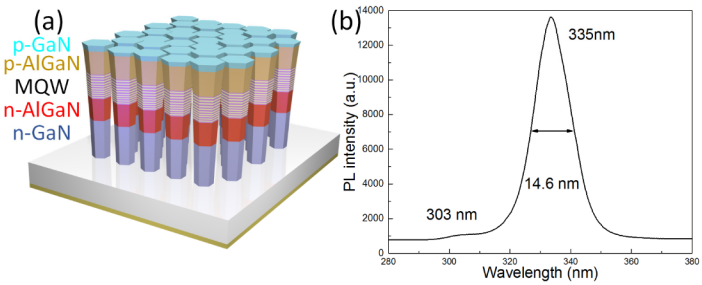

Fig. 2. (a) 3D depiction of the UV NWs LED grown on Ti/Si template substrate. (b) RTPL spectrum, with peak intensity at 303 nm and 335 nm emitted from the barrier and quantum disk using 266 nm as the excitation source.

To gain insight into the useful radiative recombination dynamics of the grown structures, it is important to understand the strength of the active medium emission. The strong PL intensity is an indication of the quantum confinement in Qdisk structures with good AlGaN crystalline quality. As shown in Fig. 2(b), the PL spectrum consists of two peaks. The two peaks located at ~303 and ~335 nm come from carrier recombination in the barrier layer and the Qdisks respectively. The emission from the active region has an FWHM of 14.63 nm which correlates to homogenous NWs and uniform Qdisks with strong confinement. In comparison UV devices using double heterostructure (DHS) have shown to have linewidth up to 30 nm thus signifying the use of quantum confined structures in the active region [20].

To study the carrier behavior in such quantum confined structures, 1D band modeling was performed using the nextnano^3 software under forward bias condition. Strain was first calculated using the built-in strain-minimization model on a free-standing NWs. This is considered, as the free surface of the NWs side-wall facilitates elastic strain relaxation [38, 39]. For example, it is noted that for SiGe/Si nanostructures up to 65% of strain relaxation has been reported [40]. The growth direction dictates the orientation of the polarization fields and in turn the band bending. In the simulation, the growth direction was taken to be N-polar. Figure 3(a) shows the calculated band diagram of the AlGaN-Qdisks-based UV NWs-LED under forward bias of 3.5 V. Figure 3(b) showed considerably large wavefunctions overlap of 42% for electrons and holes, because of the reduced piezo-polarization fields depicted in Fig. 3(c). The band offsets $\Delta E_c/\Delta E_v$ were taken to be 70/30, and the calculated recombination rates in the active region showed the SRH as the dominant source of non-radiative recombination mechanism as shown in Fig. 3(d). With further increase in voltage bias, direct recombination rate is expected to surpass SRH recombination. In the presence of large number of wells, the average carrier density is considerably reduced and thus Auger recombination, being a three

Optics EXPRESS

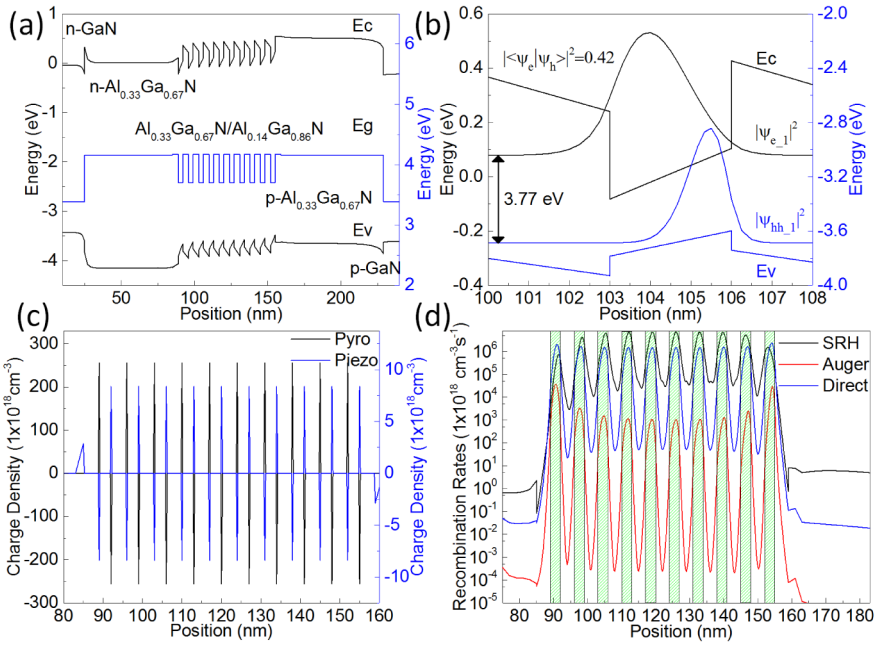

Fig. 3. (a) Band diagram, under forward bias of 3.5V. (b) Wave function profiles corresponding to electron and holes, in the active region. (c) Polarization-induced fixed charges. (d) Recombination rates including Shockley-Read-Hall (SRH), Auger and direct recombination in the active region.

particle process, is significantly suppressed. The energy separation of 3.77 eV (329 nm) between the confined carrier states correlates well with the PL and EL peak positions (335 nm and 337 nm). The energy barriers at n/p- AlGaN/GaN interfaces prevent carriers from efficiently reaching the active region. Future designs optimization based on tunnel junction and the graded layer can be adopted to improve the injection efficiency of the device.

The NWs UV LED was characterized at different DC-biases for L-I-V characteristics as illustrated in Fig. 4(a). From the I-V characteristics, it can be seen that the turn-on voltage is around 5.5 V and the series resistance is 6.68 Ω, comparable to the devices grown on Si, emitting at similar wavelengths as stated in Table 1.

Table 1. The reported UV NWs devices work with different emission wavelength and their respective onset voltages.

Wavelength (nm)	Onset Voltage (V)
207-210	*5.5-6 [18, 41, 42]*
240-280	*5-9.5 [43–46]*
280-310	*3-5 [19, 21, 47, 48]*
334-385	*3.3-7.2 [20, 22, 26, 49, 50]*

Optics EXPRESS

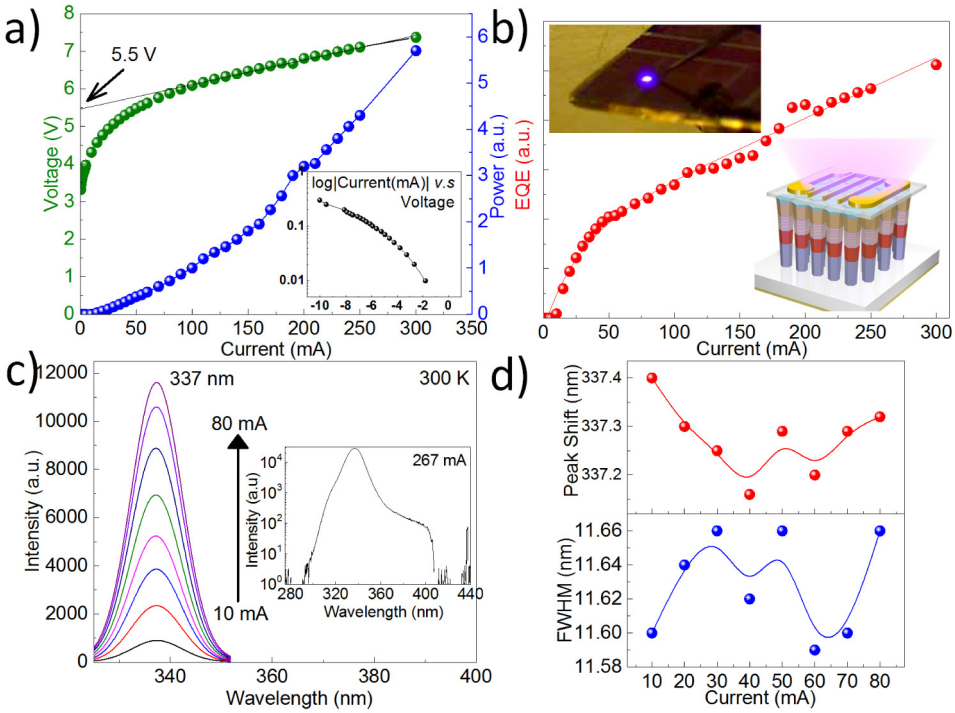

Fig. 4. (a) Current-voltage characteristics along with the measured relative optical power output. Reverse bias characteristics as an inset. (b) Relative EQE of the device with no apparent rollover up to 120 A/cm^2 with inset showing probed devices and its 3D depiction. (c) EL spectrum of nanowire device with changing current bias from 0 to 32 A/cm^2 showing an emission at 337 nm at 80 mA with inset showing negligible EL intensity around 400 nm at higher bias. (d) Peak shift and change in FWHM of EL spectrum with increase in bias current.

A significant improvement in current-voltage characteristics compared to devices grown on Si, have been shown in our prior work thus signifying the feasibility of TiN/Ti on Si substrate [25]. Also, since the polarization fields in the N-polar NWs are anti-parallel to the built-in electric fields, this contributes to relatively lower turn-on voltage. Moreover, I-V plot shows good diode characteristics with minuscule reverse leakage current as depicted in Fig. 4(a) inset compared to what's being reported (0.05 mA at –6 V) [19]. Small leakage current is an indication of a good fabrication process. Further reducing the leakage current may require avoiding the thin AlGaN shell layer via growth optimization, surface passivation, homogenizing the tilt, twist, and height of NWs and improved planarization process. An important feature to be noted is that no saturation in optical power up to 120 A/cm^2 of current injection is achieved as in Fig. 4(a). This indicates a reduced non-radiative SRH recombination in the presence of defect free active region at low injection. For high injection, previous studies on visible NWs-LEDs have shown smaller Auger recombination coefficients [51]. Though Auger recombination is expected to decrease with larger bandgap, an in-depth study is still lacking [52]. Also, better heat dissipation, excellent current injection, reduced carrier separation in the Qdisks and insignificant Auger recombination lead to the droop-free behavior up to 120 A/cm^2 for our device as shown in Fig. 4(b). External quantum efficiency (EQE) is measured by taking the ratio of the number of emitted photons over the number of injected electrons. The optical power and injection current can be derived from the L-I measurement as shown in Fig. 4(a) and the emission wavelength can be determined from the spectrum in Fig. 4(c). Figure 4(c) depicts the strong band-edge electroluminescence of the UV NWs-LED at room temperature under different dc biases. The EL peak of 337 nm at ~80 mA is close to PL peak of 335 nm at room temperature demonstrating consistency between

Optics EXPRESS

the two different excitation mechanisms and further confirming emission from the active region. A narrow linewidth of 11.7 nm is an indication of quantum confined effect and homogeneous Qdisks formation. Further LED characterization reveals that the emission peak is nearly independent on injection current and exhibits a negligible blue shift when the injection current was increased from 0 to 80 mA (see Fig. 4(d)). This suggests a weak quantum confined stark effect in the absence of strain induced piezoelectric polarization fields. In individual NWs, band filling and possible alloy broadening, as seen in PL spectra at high optical power excitation, can cause the peak to shift to shorter wavelengths [47]. A similar blue shift behavior also occurs in AlGaN quantum well based planar devices in the presence of high polarization fields [53]. However, since NWs are low polarization structures, due to lateral strain relaxation at the nucleation site, such effects are insignificant [54, 55]. No additional peak from GaN is an indication of reduced carrier leakage in the presence of efficient radiative recombination. Also, a weak ~400 nm peak, see inset in Fig. 4(c), commonly attributed to recombination via trap states introduced by Mg dopant in p-GaN, thus support the above argument [23].

4. Conclusions

In summary, the droop-free AlGaN-Qdisks-based UV-NWs-LED emitting at 337 nm was demonstrated on scalable Ti/Si template substrate. The vertically aligned NWs were grown using PAMBE with density, diameter and length of ~$9x10^{-9}$ cm^{-2}, ~80 nm, and ~350 nm respectively. TEM analysis showed well defined, defect-free Qdisks formation. Large carrier wavefunctions overlap of 42% and narrow linewidth of 11.7 nm was obtained in the presence of Qdisks. Both FWHM and peak wavelength of EL emission were invariant to injection current. The power shows no-rollover with injection current up to 120 A/cm^2 emphasizing the active role of Qdisks to reduce carrier separation and Ti interlayer which provides higher UV reflection, better heat dissipation, and improved current injection. Thus the droop-free characteristics of UV Qdisk-in-NW device reported here provided the desirable eco-friendly, and cost-saving solution for replacing mercury-based lamp for a plethora of applications.

Funding

King Abdulaziz City for Science and Technology (KACST), Grant (No. KACST TIC R2-FP-008); King Abdullah University of Science and Technology (KAUST) baseline funding, (BAS/1/1614-01-01, BAS/1/1664-01-01).